Available online at www.sciencedirect.com
SCIENCE DIRECT®
Journal of Solid State Chemistry 179 (2006) 928–934
JOURNAL OF SOLID STATE CHEMISTRY
www.elsevier.com/locate/jssc

Room-temperature synthesis and conductivity of the pyrochlore type $Dy_2(Ti_{1-y}Zr_y)_2O_7$ $(0 \leqslant y \leqslant 1)$ solid solution

Karla J. Moreno[a], Manuel A. Guevara-Liceaga[a], Antonio F. Fuentes[a,*], Javier García-Barriocanal[b], Carlos León[b], Jacobo Santamaría[b]

[a]*Cinvestav-Saltillo, Apartado Postal 663, 25000-Saltillo, Coahuila, México*
[b]*GFMC, Dpto. Física Aplicada III, Universidad Complutense de Madrid, 28040 Madrid, Spain*

Received 5 October 2005; received in revised form 22 November 2005; accepted 11 December 2005
Available online 20 January 2006

Abstract

Different compositions in a solid solution of general formula $Dy_2(Ti_{1-y}Zr_y)_2O_7$, showing high oxygen ion conductivity, have been successfully prepared at room temperature via mechanochemical synthesis. Stoichiometric mixtures of the constituent oxides were dry milled together in a planetary ball mill by using zirconia vials and balls. Chemical changes in the powder mixtures as a function of composition and milling time were followed by X-ray diffraction and revealed that, in all cases and after milling for 19 h, the powder mixtures consisted of a single phase. Electrical properties were measured on sintered pellets as a function of frequency, temperature and zirconium content, revealing an increase in conductivity of more than one order of magnitude for $y \geqslant 0.4$, which, as observed in the similar $Y_2(Ti_{1-y}Zr_y)_2O_7$, has been related with the onset of disordering of the anion sublattice. Despite increasing structural disorder with increasing Zr content, conductivity remains almost constant for $y > 0.6$, reaching a maximum value of $\sim 5 \times 10^{-3}$ for $Dy_2Zr_2O_7$ at 900 °C.

Keywords: Pyrochlores; Mechanochemical synthesis; Ionic conduction; Dysprosium titanate–zirconate; Phase transition

1. Introduction

A large number of ceramic materials have been proposed as solid oxide ion conductors and applied in devices such as solid oxide fuel cells and oxygen sensors. Among these, $A_2B_2O_7$ pyrochlore type of oxides have gained considerable attention because some of them show ionic conductivity values at high temperatures, of the same order of magnitude as those of yttria stabilized zirconia (YSZ) [1]. The fully ordered ideal pyrochlore shows cubic symmetry (SG: $Fd\bar{3}m$), and can be described in terms of a superstructure of the ideal defect fluorite structure (cubic, SG: $Fm\bar{3}m$) with twice the cell constant, $a \approx 10$ Å [2]. The basic difference between both atomic arrangements is that vacancies are randomly distributed throughout the anion sublattice in fluorites, while ordered in particular sites in "ideal pyrochlores". Thus, fully ordered pyrochlores such as $Gd_2Ti_2O_7$ are poor ionic conductors. However, high oxygen mobility can be achieved in pyrochlores by disordering the cation and anion sublattices so that disordered or "defect pyrochlores", such as $Gd_2Zr_2O_7$, are intrinsic fast oxygen conductors. Interestingly enough, different degrees of disorder can be obtained in solid solutions systems by using appropriate substitutions on the A and B sites [3]. Two solid solutions, in particular with Ti^{4+} and Zr^{4+} occupying simultaneously the 6-coordinated position, have attracted much attention: $Y_2(Ti_{1-y}Zr_y)_2O_7$ and $Gd_2(Ti_{1-y}Zr_y)_2O_7$. Neutron diffraction studies carried out in $Y_2(Ti_{1-y}Zr_y)_2O_7$ revealed a progressive disordering and phase transition as zirconium content increases, from ordered pyrochlores $(0 \leqslant y < 0.3)$ to disordered pyrochlores $(0.3 \leqslant y < 0.9)$ and anion-deficient fluorites $(y \geqslant 0.9)$ [4]. The onset of the anion sublattice disordering for $y = 0.3$ brings about a three orders of magnitude increase in the ionic conductivity of the solid solution [5]. A similar conductivity behavior has been observed in $Gd_2(Ti_{1-y}Zr_y)_2O_7$ when $y \geqslant 0.3$ [5,6], although

*Corresponding author. Fax: +52 8444389625.
E-mail address: antonio.fernandez@cinvestav.edu.mx (A.F. Fuentes).

0022-4596/$ - see front matter © 2005 Elsevier Inc. All rights reserved.
doi:10.1016/j.jssc.2005.12.015

in this solid solution there is no phase transformation to an anion-deficient fluorite type of structure since both, $Gd_2Ti_2O_7$ and $Gd_2Zr_2O_7$, are pyrochlores, the latter becoming fluorite when fired above 1500 °C. In this work, we will present the synthesis and electrical properties of a solid solution, $Dy_2(Ti_{1-y}Zr_y)_2O_7$, structurally similar to $Y_2(Ti_{1-y}Zr_y)_2O_7$; since $Dy_2Ti_2O_7$ is an ordered pyrochlore and $Dy_2Zr_2O_7$ an anion-deficient fluorite, the same structural evolution observed in $Y_2(Ti_{1-y}Zr_y)_2O_7$ should be expected in this case as the Zr content increases. Mechanical milling, which has been already successfully used for the synthesis of this type of compounds [7–10], was the method selected to prepare the samples analyzed in this work. Materials prepared by this method sometimes present non-equilibrium structures with highly disordered lattices, large number of structural defects and vacancies, all of them playing an important role in ionic mobility in solid electrolytes.

2. Experimental procedure

Seven compositions of general formula $Dy_2(Ti_{1-y}Zr_y)_2O_7$ ($0 \leqslant y \leqslant 1$) were prepared by mechanical milling, starting from mixtures of high-purity cubic Dy_2O_3 (Aldrich Chem. Inc., 99.99%), anatase TiO_2 (Aldrich Chem. Inc., 99.9 + %) and monoclinic ZrO_2 (Aldrich Chem. Inc., 99.99%). Appropriate amounts of the constituent oxides as required by stoichiometry were weighed out, mixed and ball milled together in 125-ml zirconia containers with six 20-mm-diameter zirconia balls (mass per unit $\approx$ 24 g) so as to keep balls-to-powder mass ratio equal to 10:1. Milling was performed in air at room temperature, in a Retsch PM/400 planetary ball mill, using a rotating disc speed of 350 rpm and reversed rotation every 20 min. Phase evolution on milling was followed using X-ray powder diffraction (XRD) on a Philips X'pert diffractometer using Ni-filtered Cu$K\alpha$ radiation ($\lambda = 1.5418$ Å). Ball-milled powders were also examined by scanning electron microscopy (SEM) in a Philips XL30 ESEM microscope equipped with an EDAX Inc. energy-dispersive X-ray detector for microanalysis.

Impedance studies were carried out from 350 to 900 °C (50 °C steps) on pellets (10 mm diameter and ~1 mm thickness) obtained by uniaxially pressing (1500 MPa) the fine-milled powders obtained by milling. To increase their mechanical strength and obtain dense samples, pellets were sintered at 1500 °C for 36 h (heating and cooling rates 2 °C min^{-1}). AC impedance measurements were carried out in air using a Solartron 1260 Frequency Response Analyzer over the 100 Hz to 1 MHz frequency range. Electrodes were made by coating opposite faces of the pellets with SPI-Chem™ conductive platinum paint and firing them at 800 °C to eliminate the organic components and harden the Pt residue. The phase purity of the pellets was analyzed by XRD and cell parameters calculated by the Rietveld method using the FullProf program [11].

3. Results and discussion

3.1. Synthesis and characterization

Fig. 1 shows an XRD study of the evolution of two compositions in the $Dy_2(Ti_{1-y}Zr_y)_2O_7$ solid solution, selected as representatives of the series, with milling time. While Fig. 1a shows the evolution of the ($Dy_2O_3 + 2TiO_2$) starting mixture, Fig. 1b shows that of the ($Dy_2O_3 + 2ZrO_2$) mixture. A common feature observed in all powder patterns after milling for 1 h is a significant decrease in intensity and broadening of the characteristic diffraction peaks of the starting oxides as a result of the strong decrease of crystallite size and increase in lattice strain. During milling, powder particle size decreases rapidly with

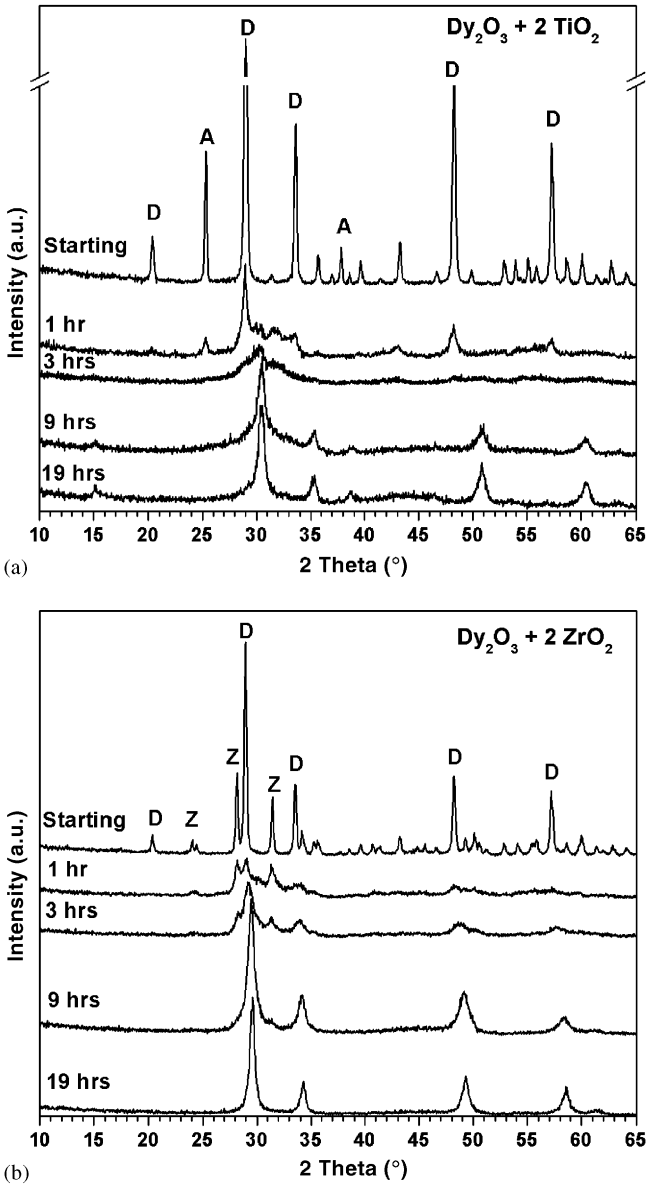

Fig. 1. Evolution of the (a) ($Dy_2O_3 + 2TiO_2$) and (b) ($Dy_2O_3 + 2ZrO_2$) mixtures with milling time. Z, A and D stand for monoclinic ZrO_2, anatase TiO_2 and cubic Dy_2O_3, respectively.

time and reaches a small value just after only a few minutes. As Fig. 1a shows, ball milling also induces the Dy_2O_3 polymorphic transformation, from the highly symmetric cubic form present in the initial powder mixture, the so-called C-form in lanthanide (III) oxides, to the monoclinic B-form, as evidenced by the evolution of new reflections in the 29–33° region (2θ). This transformation, which is normally temperature driven, taking place when cubic Dy_2O_3 is fired at temperatures above 1800 °C, can be also caused by the application of very high pressures or high-energy milling [12]. While the macroscopic temperature of the vial (or powder) has been measured by different authors and found to be commonly between 100 and 120 °C, determining the local (microscopic) temperature during milling raises important technical difficulties [13]. This temperature is normally estimated indirectly by, for example, observing the crystal structure changes during milling, or calculated by using some more or less complex, theoretical models. In any case, modest rises with temperatures not higher than 500 °C are normally predicted, well below that reported for the C- to B-Dy_2O_3 transformation. On the other hand, the average pressure experienced by powder particles trapped in collisions during mechanical milling in planetary ball mills is believed to be as high as ~6 GPa [14]. The combined action of local temperature and pressure acting repeatedly on powder particles for times of the order of the microseconds makes mechanical milling a unique tool for developing non-equilibrium materials. Thus, metastable phases existing at equilibrium only at high temperatures and/or high pressures such as B-Dy_2O_3 are commonly present in powder mixtures subject to mechanical milling. Monoclinic Dy_2O_3 seems to be the predominant form in our powder mixture when milling time increases to 3 h. The {101} line of anatase, still present after 1 h, is no longer observable after milling for 3 h. The powder milled for 9 h shows an XRD pattern containing the characteristic reflections of the end product, cubic $Dy_2Ti_2O_7$ (PDF:17-0453), with further milling (19 h) increasing the intensity of its characteristic reflections.

Identification of chemical species after the initial hour milling period shown in Fig. 1b is difficult because of overlapping reflections. However, some strong additional reflections are evident after milling for 3 h, with increasing intensity as milling progresses to the point that, after 9 h, the XRD pattern obtained resembles that typical of a fluorite-like structure. As already mentioned, the pyrochlore structure can be considered as a superstructure of an anion-deficient fluorite-like atomic arrangement with twice the cell constant. Therefore, its diffraction pattern contains a set of strong intensities characteristic of the underlying fluorite-type average structure plus an additional set of superstructure reflections, with intensities depending on factors such as the degree of ordering, difference in average scattering factors of the elements involved, distribution of oxygen vacancies, etc. [4]. Powder patterns collected after milling for 9 and 19 h clearly indicate the formation of a reaction product although none of the superstructure reflections typical of pyrochlores are observed, suggesting therefore the formation of a highly disordered product. The above-mentioned observations suggest that the mechanically activated chemical reaction between Dy_2O_3, TiO_2 and/or ZrO_2 involves an initial step of particle size reduction of the constituent oxides, together with the introduction of a large number of crystal defects and the polymorphic transformation of Dy_2O_3, from that of cubic symmetry to the lower symmetric monoclinic form. The formation of the $Dy_2(Ti_{1-y}Zr_y)_2O_7$ phases takes place as a second step and is evident after milling for only 3 h.

All seven compositions studied in this work were prepared by milling stoichiometric mixtures of the constituent oxides for 19 h, as described above, giving white-colored reaction products. Fig. 2a shows a comparison

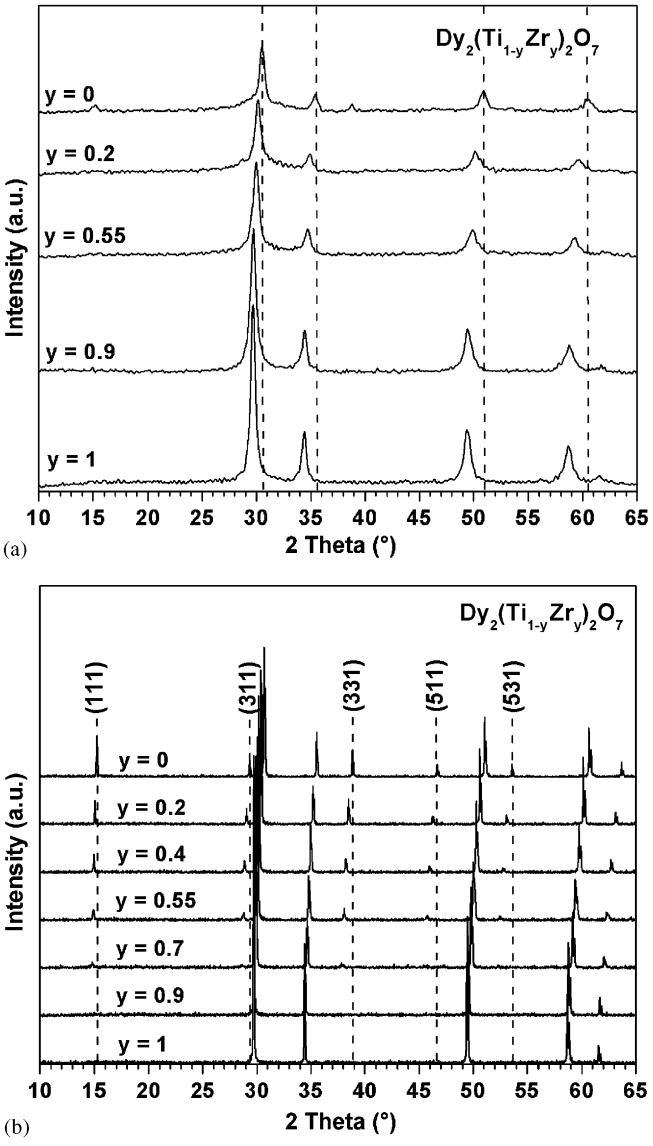

Fig. 2. Comparison between the XRD patterns of powder mixtures just milled (a) and milled and fired at high temperatures (b) with different Ti/Zr ratios; vertical lines are only shown to emphasize structural changes as zirconium content increases.

between the XRD patterns of five compositions with different Ti^{4+}/Zr^{4+} ratios (decreasing from top to bottom). Although the superstructure reflections typical of pyrochlores are barely evident only in pure $Dy_2Ti_2O_7$ (e.g. the {111} and {331}lines at $2\theta = 15.28^\circ$ and 38.99°, respectively), there is a marked shift in the position of all reflections observed towards low angles (increasing as the zirconium content increases), suggesting an increase in cell size. This is an obvious consequence of the substitution of Ti^{4+} by a larger cation, Zr^{4+} (0.60 vs. 0.72 Å, both in octahedral coordination) [15], and confirms the formation of the title solid solution on milling. Fig. 2b shows the XRD patterns of all seven compositions prepared in this work after firing them, 12 h at 1450 °C. Two effects are obvious as the zirconium content increases. Firstly, the intensity of the characteristic reflections of the pyrochlore superstructure decreases (disordering increases) although they are evident for at least $y \leqslant 0.7$ (y values in $Dy_2(Ti_{1-y}Zr_y)_2O_7$), suggesting this as the upper stability limit of the pyrochlore-type solid solution. Secondly, cell size increases as Zr^{4+} increases.

Some doubts have been raised over the real stability limits of both solid solutions in $Y_2(Ti_{1-y}Zr_y)_2O_7$. In fact, and based on XRD and high-resolution transmission electron microscopy data, a recent study establishes new stability limits for the pyrochlore-type ($0 \leqslant y \leqslant \sim 0.54$) and for the defect fluorite-type solid solutions ($\sim 0.68 \leqslant y \leqslant 1$) and proposes the existence of a two-phase region between them [16]. Differences between this study and that of Heremans et al., already mentioned here, were related to the exceptionally slow cation diffusion in fluorite-related stabilized zirconia systems, which makes it difficult to reach equilibrium single-phase samples. Long firing cycles (between 5 and 20 days) at temperatures higher than 1350 °C were used in the latter study. An in-depth structural study of the $Dy_2(Ti_{1-y}Zr_y)_2O_7$ solid solution is currently under way in this group. However, for the purposes of this work, samples were satisfactorily modeled as pyrochlores up to a zirconium content of $y = 0.7$, while the composition of nominal formula $Dy_2(Ti_{0.1}Zr_{0.9})_2O_7$, was attempted with both fluorite and pyrochlore structures, giving better results as the former and therefore excluding the existence of long-range atomic ordering for the anion and cation sublattices. Fig. 3 shows the evolution of cell parameters of the series with zirconium content, which is in apparent agreement with Vegard's law ($a(Å) = 10.1366 + 0.3175y$). Fig. 4 shows a SEM micrograph of the $Dy_2(Ti_{0.8}Zr_{0.2})_2O_7$ composition, sintered at 1500 °C. A fully densified microstructure, free of porosity, was observed for the samples rich in titanium, with slightly increasing porosity as the zirconium content increases.

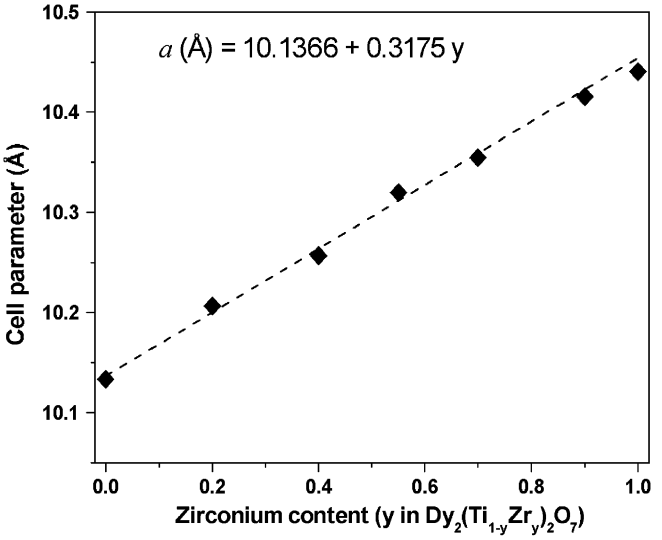

Fig. 3. Variation of cell size with zirconium content for the $Dy_2(Ti_{1-y}Zr_y)_2O_7$ ($0 \leqslant y \leqslant 1$) solid solution. Values plotted for compositions of nominal formula $Dy_2(Ti_{0.1}Zr_{0.9})_2O_7$ and $Dy_2Zr_2O_7$ are twice the lattice constant of the defect fluorite and were excluded from the linear fit.

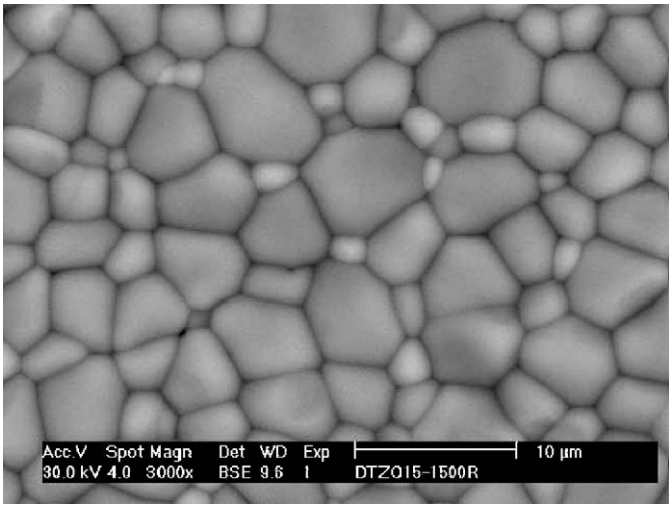

Fig. 4. SEM micrograph of the $Dy_2(Ti_{0.8}Zr_{0.2})_2O_7$ composition sintered at 1500 °C as described in the experimental section, showing a complete absence of pores.

3.2. Conductivity measurements

Fig. 5a shows the frequency dependence of the real part of the conductivity at different temperatures for a composition, $Dy_2(Ti_{0.45}Zr_{0.55})_2O_7$, selected as representative of the series; similar plots were obtained for all compositions analyzed in this work. At the lowest temperatures, 350 and 400 °C, the conductivity shows a Jonscher-type power law [17] frequency dependence at high frequencies, followed by a frequency-independent plateau associated to the dc conductivity regime, and finally a conductivity decrease at low frequencies due to blocking effects at grain boundaries. At higher temperatures, between 450 and 600 °C, a second plateau arises at low frequencies due to the grain boundary contribution to the conductivity. The difference between the bulk dc conductivity and the grain boundary conductivity decreases with increasing temperature, and above 700 °C the value of the grain boundary conductivity becomes higher than that

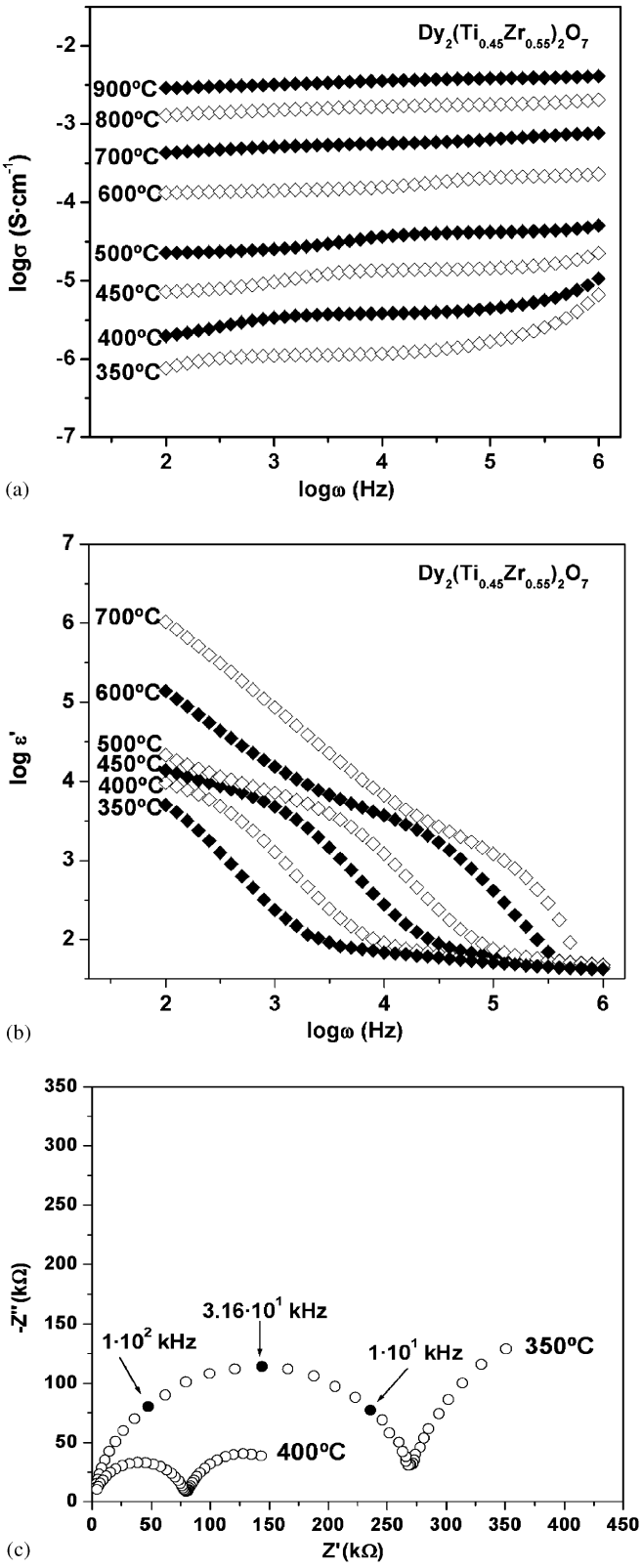

Fig. 5. The frequency dependence of the real parts of (a) conductivity and (b) permittivity, and (c) complex impedance plots of $Dy_2(Ti_{0.45}Zr_{0.55})_2O_7$ at different temperatures.

of the bulk dc conductivity. It can be also observed in the same figure the blocking effect at the electrodes, showing up as a decrease of the conductivity at low frequencies at the highest temperatures (above 700 °C). This is a clear indication that the conductivity is ionic. Fig. 5b shows the real part of the dielectric permittivity as a function of frequency and temperature for the same composition. The high frequency permittivity value was found to be $\varepsilon_\infty = 37 \pm 7$, almost independent of temperature and composition. The increase observed at low frequencies is due to blocking effects. Note that these blocking effects arise at frequencies below 1 MHz even at 700 °C, the highest temperature. This means that the conductivity at the highest frequencies in Fig. 5a is always dominated by the bulk contribution, even at the highest temperature. Blocking effects at low frequencies are also evident in Fig. 5c, which shows complex impedance plots obtained at 350 and 400 °C for the same composition. Two semicircles can be observed at each temperature, related to the bulk and grain boundary contributions at high and low frequencies, respectively.

Either from the conductivity value at the high-frequency plateau in Fig. 5a, or from the conductivity value between the semicircles in Fig. 5c, the bulk dc conductivity is easily obtained from experimental data. Fig. 6a shows the evolution of the dc conductivity with zirconium content and temperature for the whole solid solution. A high increase in conductivity of more than one order of magnitude is observed for all temperatures when $y = 0.4$, remaining almost independent from the zirconium content for compositions with $y > 0.6$. Interesting enough, a similar conductivity behavior was observed for the already-mentioned $Y_2(Ti_{1-y}Zr_y)_2O_7$ solid solution, and was related with the onset of anion disordering as the zirconium content increases. Progressive structural disorder in $A_2B_2O_7$ pyrochlores takes place as the R_A to R_B ratio approaches unity, with the conduction mechanism proposed for defect pyrochlores being still the subject of some controversy. Using computing simulation techniques, van Dijk et al. [18] proposed oxygen Frenkel defects of the type 48*f* vacancy and 8*b* interstitial as the most stable intrinsic defects to be present in $Gd_2Zr_2O_7$ requiring 1.96 eV per defect. In fact, they predicted for pyrochlores an actual defect structure consisting of "split vacancies", a 48*f* vacancy pair in the ⟨110⟩ direction with an interstitial ion in between, a scenario slightly more stable (by 0.2 eV) than a single 48*f* vacancy. A diffusion mechanism consisting of sequential jumps of oxygen atoms along the 48*f* sites, either between (i) nearest neighbor sites (along ⟨100⟩) and/or (ii) along ⟨110⟩ involving the "split vacancy" structure (next nearest neighbor), was proposed as responsible for the migration of vacancies. In a more recent work, Pirzada et al. examined the 48*f* vacancy configuration for a large number of $A_2B_2O_7$ compounds (A = Lu to La, B = Ti to Pb), concluding that the "split vacancy" configuration proposed by van Dijk et al. becomes more stable with respect to the single vacancy, as the pyrochlore to fluorite phase boundary is approached (when the R_A/R_B ratio comes close to 1), that is, for highly disordered pyrochlores [19]. According to their

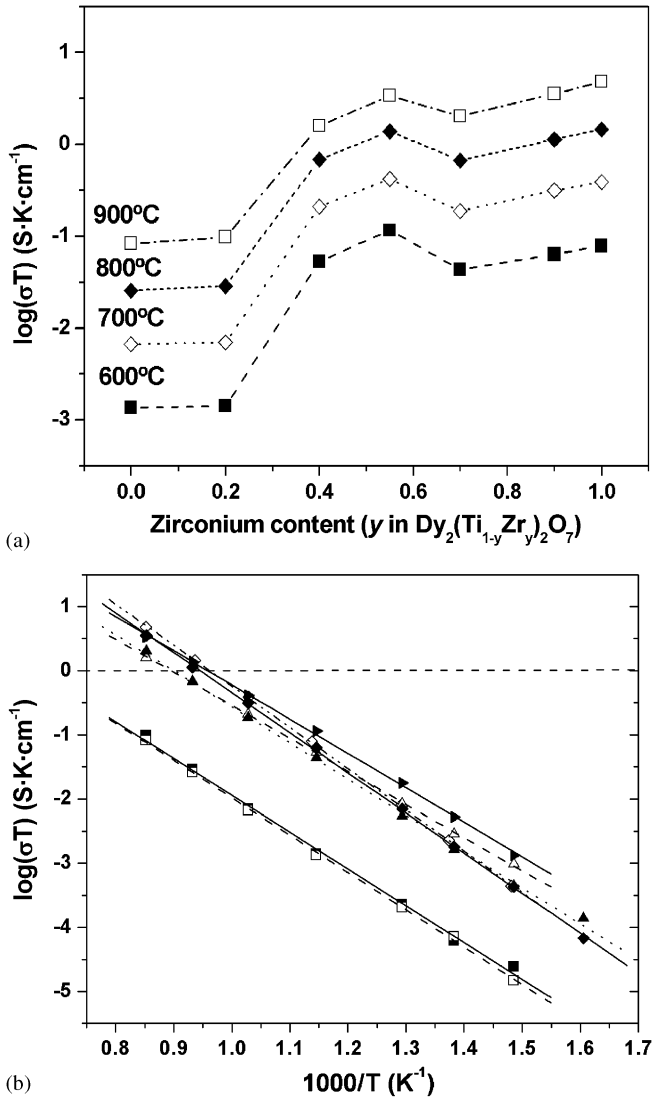

Fig. 6. (a) Conductivity as a function of Zr content and temperature and (b) Arrhenius plots of dc conductivity for $Dy_2(Ti_{1-y}Zr_y)_2O_7$ ($0 \leqslant y \leqslant 1$); dotted lines in (a) are only drawn to show trends. For (b), $y = 0$ (□), 0.2 (■), 0.4 (△), 0.55 (►), 0.7 (▲), 0.9 (♦) and 1 (◇).

calculations, for compounds which do not exhibit "split vacancy" formation, all oxygen ion jumps will be along the ⟨100⟩ direction, while for those who do the overall mass transport would be much more complex and not along the ⟨100⟩ direction but on average, along the ⟨111⟩ direction. The "split vacancy" configuration provides greater geometrical flexibility and longer effective jump distances, making additional contributions and enhancing the ionic mobility as disorder increases. The existence of the "split vacancy" configuration has been experimentally proved by Chen et al. using X-ray photoelectron spectroscopy [20].

The highest conductivity value for this solid solution, $4.7 \times 10^{-3}\,S\,cm^{-1}$ at 900 °C, is reached for $Dy_2Zr_2O_7$, which exhibits an anion-deficient fluorite type of structure. This value is similar to that measured for $Y_2Zr_2O_7$ ($\sim 5 \times 10^{-3}\,S\,cm^{-1}$) at the same temperature, and below

Table 1

Zr content y in $Dy_2(Ti_{1-y}Zr_y)_2O_7$	Pre-exponential factor ($S\,K\,cm^{-1}$)	E_a (eV)
0	6.8×10^3	1.151
0.2	6.2×10^3	1.135
0.4	4.0×10^4	1.019
0.55	1.3×10^5	1.062
0.7	1.2×10^5	1.115
0.9	8.0×10^5	1.237
1	14.8×10^5	1.270

that reported for $Gd_2Zr_2O_7$ ($\sim 10^{-2}\,S\,cm^{-1}$) [5]. The temperature dependence of the dc conductivity was analyzed by using an Arrhenius law of the form: $\sigma_{dc} \times T = \sigma_o \exp(-E_a/k_B T)$, where σ_o is the pre-exponential factor (which is related to the effective number of mobile species) and E_a denotes the activation energy for the conduction process. Fig. 6b shows such representations for each composition studied in this work where the lines are fits to an Arrhenius law, confirming that the ionic diffusion process is thermally activated. The activation energy and pre-exponential factor for each composition were calculated from the slopes and intercept, respectively, of the linear fits, and are presented in Table 1. The activation energy found for the series are included within the 1.14 ± 0.12 eV interval, similar to those reported for the $Y_2(Ti_{1-y}Zr_y)_2O_7$ solid solution, 1.1–1.3 eV, but higher than the ~0.85 eV observed for its similar with Gd^{3+} instead of Dy^{3+} [5]. Pre-exponential factors within the series were found to increase substantially, with Zr content reaching a value of $14.8 \times 10^5\,S\,K\,cm^{-1}$ for $Dy_2Zr_2O_7$, although this fact does not translate into higher conductivity. Increasing disorder (increasing the Zr^{4+} content) increases the pre-exponential factor (therefore, the number of mobile species), but it also increases the activation energy needed for the mobile species to migrate, resulting in conductivity remaining almost constant when $y > 0.6$. Cooperative effects in oxygen hopping dynamics have been shown to be a key factor in determining ionic conductivity values in a similar system, $Gd_2(Ti_{1-y}Zr_y)_2O_7$ [21]. Increasing the concentration of mobile species results in larger cooperativity and consequently in higher activation energies for long-range ion transport.

4. Conclusions

Several compositions in the $Dy_2(Ti_{1-y}Zr_y)_2O_7$ solid solution were successfully prepared at room temperature, by ball milling at a moderate rotating speed stoichiometric mixtures of high-purity oxides. The XRD patterns of powder samples annealed at high temperatures show an increase in disordering as the Zr^{4+} content increases, denoted by the decrease in the intensity of the superstructure reflections typical of pyrochlores. The onset of disordering is also evidenced by the increase of almost two

orders of magnitude in conductivity values when $y > 0.4$, reaching a maximum of $\sim 5 \times 10^{-3}$ at 900 °C for $Dy_2Zr_2O_7$.

Acknowledgments

This work has been carried out with the financial assistance of CONACYT (SEP-2003-C02-44075) and CAM (GR/MAT/0250/2004). Helpful discussions with U. Amador are greatly appreciated.

References

[1] J. Burgraaf, T. van Dijk, M.J. Verkerk, Solid State Ion. 5 (1981) 519–522.
[2] M. Subramanian, G. Aravamudan, G.V. Subba Rao, Prog. Solid State Chem. 15 (1983) 55–143.
[3] B.J. Wuensch, K.W. Eberman, C. Heremans, E.M. Ku, P. Onnerud, E.M.E. Yeo, S.M. Haile, J.K. Stalick, J.D. Jorgensen, Solid State Ion. 129 (2000) 111–133.
[4] C. Heremans, B.J. Wuensch, J.K. Stalick, E. Prince, J. Solid State Chem. 117 (1995) 108–121.
[5] P.K. Moon, H.L. Tuller, Mater. Res. Soc. Symp. Proc. 135 (1989) 149–163.
[6] P.K. Moon, H.L. Tuller, Solid State Ion. 28–30 (1988) 470–474.
[7] L.B. Kong, J. Ma, W. Zhu, O.K. Tan, J. Alloys Comp. 335 (2002) 290–296.
[8] K.J. Moreno, R.S. Rodrigo, A.F. Fuentes, J. Alloys Comp. 390 (2005) 230–235.
[9] A.F. Fuentes, K. Boulahya, M. Maczka, J. Hanuza, U. Amador, Solid State Sci. 7 (2005) 343–353.
[10] E.V. Tsipis, A.V. Shlyakhtina, L.G. Shcherbakova, I.V. Kolbanev, V.V. Kharton, N.P. Vyshatko, J.R. Frade, J. Electroceram. 10 (2003) 153–164.
[11] J. Rodriguez-Carvajal, FULLPROF program. Abstracts of the Satellite Meeting on Powder Diffraction of the XVth Congress of the IUCr, Toulouse, France, 1990, p. 17.
[12] D. Michel, L. Mazerolles, P. Berthet, E. Gaffet, Eur. J. Solid State Inorg. Chem. 32 (1995) 673–682.
[13] C. Suryanarayana, Prog. Mater. Sci. 46 (2001) 1–184.
[14] J. Alkebro, S. Bégin-Colin, A. Mocellin, R. Warren, J. Solid State Chem. 164 (2002) 88–97.
[15] R.D. Shannon, Acta Crystallogr. A 32 (1976) 751–767.
[16] Y. Liu, R.L. Withers, L. Norén, J. Solid State Chem. 177 (2004) 4404–4412.
[17] A.K. Jonscher, Dielectric Relaxation in Solids, Chelsea Dielectric Press, London, 1983.
[18] M.P. van Dijk, A.J. Burggraaf, A.N. Cormack, C.R.A. Catlow, Solid State Ion. 17 (1985) 159–167.
[19] M. Pirzada, R.W. Grimes, L. Minervini, J.F. Maguire, K.E. Sickafus, Solid State Ion. 140 (2001) 201–208.
[20] J. Chen, J. Lian, L.M. Wang, R.C. Ewing, R.G. Wang, W. Pan, Phys. Rev. Lett. 88 (2002) 105901.
[21] K.J. Moreno, G. Mendoza-Suárez, A.F. Fuentes, J. García-Barriocanal, C. León, J. Santamaría, Phys. Rev. B 71 (2005) 132301.